jove

Microembossing: A Convenient Process for Fabricating Microchannels on Nanocellulose Paper-Based Microfluidics

Wenwen Yuan[1,2,3], **Hang Yuan**[1], **Sixuan Duan**[1,2], **Ruiqi Yong**[1], **Jia Zhu**[1,2,4], **Eng Gee Lim**[1,2], **Ivona Mitrovic**[2], **Pengfei Song**[1,2]

[1] School of Advanced Technology, Xi'an Jiaotong - Liverpool University [2] Department of Electrical Engineering and Electronics, University of Liverpool [3] State Key Laboratory for Manufacturing Systems Engineering, Xi'an Jiaotong University [4] School of Intelligent Manufacturing and Smart Transportation, Suzhou City University

Corresponding Author

Pengfei Song

Pengfei.Song@xjtlu.edu.cn

Citation

Yuan, W., Yuan, H., Duan, S., Yong, R., Zhu, J., Lim, E.G., Mitrovic, I., Song, P. Microembossing: A Convenient Process for Fabricating Microchannels on Nanocellulose Paper-Based Microfluidics. *J. Vis. Exp.* (200), e65965, doi:10.3791/65965 (2023).

Date Published

October 6, 2023

DOI

10.3791/65965

URL

jove.com/video/65965

Abstract

Nanopaper, derived from nanofibrillated cellulose, has generated considerable interest as a promising material for microfluidic applications. Its appeal lies in a range of excellent qualities, including an exceptionally smooth surface, outstanding optical transparency, a uniform nanofiber matrix with nanoscale porosity, and customizable chemical properties. Despite the rapid growth of nanopaper-based microfluidics, the current techniques used to create microchannels on nanopaper, such as 3D printing, spray coating, or manual cutting and assembly, which are crucial for practical applications, still possess certain limitations, notably susceptibility to contamination. Furthermore, these methods are restricted to the production of millimeter-sized channels. This study introduces a straightforward process that utilizes convenient plastic micro-molds for simple microembossing operations to fabricate microchannels on nanopaper, achieving a minimum width of 200 µm. The developed microchannel outperforms existing approaches, achieving a fourfold improvement, and can be fabricated within 45 min. Furthermore, fabrication parameters have been optimized, and a convenient quick-reference table is provided for application developers. The proof-of-concept for a laminar mixer, droplet generator, and functional nanopaper-based analytical devices (NanoPADs) designed for Rhodamine B sensing using surface-enhanced Raman spectroscopy was demonstrated. Notably, the NanoPADs exhibited exceptional performance with improved limits of detection. These outstanding results can be attributed to the superior optical properties of nanopaper and the recently developed accurate microembossing method, enabling the integration and fine-tuning of the NanoPADs.

Introduction

Recently, nanofibrillated cellulose (NFC) paper (nanopaper) has emerged as a highly promising substrate material for various applications such as flexible electronics, energy devices, and biomedicals[1,2,3,4]. Derived from natural plants, nanopaper is cost-effective, biocompatible, and biodegradable, making it an appealing alternative to traditional cellulose paper[5,6]. Its exceptional properties include an ultra-smooth surface with a surface roughness of less than 25 nm and a dense cellulose matrix structure, allowing for the creation of highly structured nanostructures[7]. Abundant hydroxyl groups of nanopaper contribute to its compact and tightly packed nanocellulose structure[8]. Nanopaper exhibits excellent optical transparency and minimal optical haze, making it well-suited for optical sensors. Additionally, its inherent hydrophilicity enables pump-free flow, even with its thick structure, providing autonomous fluid motion[9,10]. Nanocellulose has diverse applications in biological sensors, conductive electronic devices, cell culture platforms, supercapacitors, batteries, and more, showcasing its versatility and potential[11,12]. Particularly, nanocellulose is promising for paper-based analytical microfluidic devices (μPADs), offering unique advantages over conventional chromatography paper.

In the past decade, μPADs have achieved significant attention due to their affordability, biocompatibility, pump-free operation, and ease of production[13,14]. These devices have emerged as effective point-of-care diagnostic tools, particularly in resource-limited settings[15,16,17]. A significant advancement in this field was the development of wax printing, pioneered by George Whitesides[18] and the Bingcheng Lin group[19], enabling the creation of functional μPADs by incorporating microchannels on chromatography paper. Subsequently, μPADs rapidly evolved, and various biosensing techniques, including electrochemical methods[20], chemiluminescence[21], and enzyme-linked immunosorbent assay (ELISA)[22,23,24], were successfully implemented for the detection of diverse biomarkers such as proteins[25,26], DNAs[27,28], RNAs[29,30], and exosomes[31]. Despite these achievements, μPADs still face challenges, including slow flow speeds and solvent evaporation.

Several methods have been proposed for creating microchannels on nanopaper[32,33,34]. One approach involves 3D printing sacrificial ingredients into the material, but it requires a hydrophobic coating that limits pump-free operation[33]. Another technique involves manually stacking channel layers between nanopaper sheets using glue, which is labor-intensive[32]. Alternatively, spray-coating nanocellulose fibers onto pre-patterned molds can create microchannels, but it involves time-consuming and expensive mold preparation[34]. Notably, these methods are limited to millimeter-scale microchannels, compromising the advantages of microfluidic devices regarding reagent volume consumption and integration. Developing a simple nanopaper microchannel patterning process with micrometer-scale resolution remains a challenge.

This study presents a unique nanopaper microchannel patterning method based on practical microembossing. The approach offers several advantages over existing methods, as it requires no expensive or specialized equipment, is simple, cost-effective, and highly accurate. A convex microchannel mold is fabricated by laser cutting a polytetrafluoroethylene (PTFE) film, known for its chemical inertness and nonstick properties. This mold is then used

to emboss microchannels onto a nanopaper gel membrane. A second layer of nanopaper gel is applied on top to create closed hollow channels. Using this patterning technique, fundamental microfluidic devices on nanopaper are developed, including a laminar mixer and droplet generator. Additionally, the fabrication of surface-enhanced Raman microscopy (SERS) NanoPADs is demonstrated. *In-situ* creation of a silver nanoparticle-based SERS substrate is achieved by introducing two chemical reagents ($AgNO_3$ and $NaBH_4$) into the channels, resulting in a remarkable performance with low limits of detection (LODs).

Protocol

1. Microembossing process for microchannel patterning on nanopaper

1. Mold preparation

   NOTE: Refer to Yuan et al.[12] for details on mold preparation.

   1. Prepare a PTFE film as indicated in the **Table of Materials**.
   2. Laser-cut the prepared PTFE film to make a convex microchannel mold (**Figure 1A-I**).

      NOTE: The dimensions of the PTFE mold determine the microchannel dimensions (**Figure 2E,F**) in a linear first-order function relationship.

2. Nanopaper preparation

   1. Disperse 4.0 g of (2,2,6,6-tetramethylpiperidin-1-yl)oxyl (TEMPO)-oxidized NFC gel (see **Table of Materials**) in distilled water (final concentration of 0.1 wt%).
   2. Stir the suspension heavily at 120.8 x *g* for 30 min at room temperature until no cellulose floc is visible.
   3. Vacuum-filter the clear suspension to obtain a nanopaper gel (**Figure 1A-II**).

      NOTE: In this example, the diameter of the obtained nanopaper gel is 4 cm. NanoPADs can be tailored for various applications by selecting suction filtration devices with different radii, enabling the design of NanoPADs at different scales.

3. Embossing of nanopaper gel

   1. Place the PTFE mold on the surface of the nanopaper gel.
   2. Emboss the nanopaper gel (**Figure 1A-III**) using the PTFE mold by the hot press for 10 min each time under optimized pressure and temperature (**Figure 2A-D**).

      NOTE: Higher embossing pressure (250 kPa to 1000 kPa) improves fabrication accuracy but should not exceed 1000 kPa to prevent damage to the cellulose structure. Higher embossing temperatures (25-100 °C) enhance microchannel accuracy by promoting dehydration and decarburization, but temperatures should not exceed 75 °C to avoid gel wrinkling and reduced light transmittance[7]. In this example, optimized embossing parameters were 750 kPa and 75 °C.

4. Mold releasing

   1. Peel off an additional layer of filter nanopaper gel from the filter membrane (**Figure 1A-IV**).

5. Bonding

   1. Attach the peeled layer on top of the embossed layer of nanopaper gel, stacking the two layers to create a hollow microchannel structure (**Figure 1A-V**).

NOTE: The stronger hydrogen bonding in 'gel-like' nanopaper compared to fiber suspension and dried nanopaper enhances the entanglement and adhesion of nanocellulose fibers. Consequently, two layers of 'gel-like' nanopaper can bond tightly through self-diffusion without external force.

6. Drying

    1. Place the two layers of nanopaper gel in a drying oven at 75 °C for approximately 30 min (**Figure 1A-VI**).

2. Construction of fundamental microfluidic devices

1. Construction of laminar-mixer

    1. Prepare the NanoPADs with straight and curved channels (**Figure 3A**) following step 1.

        NOTE: In this example, the dimensions of channels are 1 mm width and 50 µm depth.

    2. Add red and blue droplets in the inlet zones simultaneously, allowing flow through the hollow channel automatically.

        NOTE: The successful independent flow of the red and blue solutions in a straight channel and their mixing at the end of the curved channel can be attributed to the low Reynolds number of the layers in microfluidic devices and the radial flow induced by shear stress[35].

2. Construction of droplet generator

    1. Prepare the two-inlet NanoPADs with a T-junction channel (**Figure 3D**) according to step 1.

    2. Introduce water and hexadecane (oil), two immiscible liquids, into the two-inlet zones of the T-junction channel to generate droplets (**Figure 3E**).

        NOTE: In this example, the dimensions of the T-junction channel are 1 mm width, 25 mm length, and 50 µm depth.

    3. Fix the speed of Q_1 at 6 µL/min, and the speed of Q_2 at n × Q_1 (n = 1-6). Use two syringe pumps and set them at the above speed to inject water and oil. This behavior is governed by the one simple scaling equation (provided below).

        NOTE: In this example, oil and colored water were poured into the channel[36].

        $$\frac{L}{W} = \alpha + \beta\frac{Q_1}{Q_2}$$

        Where α = 1, β = 1, L is the length, W is the width of the droplet, and Q_1 and Q_2 are the flow rates of water and hexadecane, respectively[37,38].

3. *In-situ* AgNP growth

1. NanoPADs preparation

    1. Prepare two-inlet NanoPADs with a converging detection zone (**Figure 4A**) according to step 1.

2. Successive ionic layer adsorption and reaction process

    1. Prepare a 20 mM $AgNO_3$ solution and a 20 mM $NaBH_4$ solution (see **Table of Materials**).

    2. Drop 5 µL of the 20 mM $AgNO_3$ solution into the left inlet zone of the flow channel.

    3. Allow the $AgNO_3$ solution to remain in the reaction zone for 30 s.

        NOTE: Repeat steps 3.2.2. and 3.2.3. five times to ensure the uniform distribution of AgNPs without agglomeration, which could explain the higher band intensity.

4. Drop 5 µL of distilled water into the left inlet zone of the flow channel for rinsing.

   NOTE: Repeat step 3.2.4. three times to ensure the removal of excessive, unadsorbed Ag ions through washing.

5. Add 5 µL of the 20 mM $NaBH_4$ solution to the right inlet zone of the flow channel.

   NOTE: Repeat step 3.2.5. until the AgNPs are generated evenly in the reaction zone. The chemical reactions involved in step 3 are represented by the following formula[39]:

   $$AgNO_3 + NaBH_4 \rightarrow Ag + \frac{1}{2}H_2 + \frac{1}{2}B_2H_6 + NaNO_3$$

   In this example, dense, uniform, well-structured AgNP arrays were formed on the NanoPADs (**Figure 4B**). The average diameter of the AgNPs was 55 nm (**Figure 4C**).

4. SERS measurement

1. Raman spectroscopy system preparation

   1. Turn on the laser and launch the accompanying software for the Raman spectrometer (see **Table of Materials**).

   2. Employ a 50x objective for focusing and collecting Raman signals and a 532 nm laser for excitation.

   3. Set the spectral resolution to 2 cm^{-1} for accurate measurement. Set Raman spectrum measurement range from 400 cm^{-1} to 600 cm^{-1}.

   4. Calibrate the Raman spectrometer using a silicon wafer[12].

      NOTE: Perform step 4.1. for step 4.2.

2. Rhodamine B (RhB) measurement

   1. Dissolve 4.7 mg of RhB (see **Table of Materials**) in 10 mL of ethanol to prepare a 1 mM RhB solution.

   2. Prepare a series of RhB solutions with concentrations ranging from 10 µM to 0.1 pM by diluting the 1 mM RhB solution in the ethanol.

   3. Add 5 µL of the RhB solution onto the inlet zone of the NanoPADs channel and let it dry.

      NOTE: Repeat step 4.2.3. for RhB solutions of different concentrations indicated in step 4.2.2.

   4. Set the excitation time to 10 s, the grating to 2 cm^{-1}, and the number of cycles to 1. Set Raman spectrum measurement range from 500 cm^{-1} to 1800 cm^{-1}.

   5. Adjust the coarse focus screw and fine focus screw individually to achieve proper focus, then click on **stop** to save the position.

   6. Click on **start** to begin the measurement.

   7. Repeat the measurements seven times and save the collected data.

   8. Turn off the laser.

3. Data analysis

   1. Import the saved data into the data analysis software (see **Table of Materials**).

   2. Calculate the average spectrum from the saved data.

   3. Select the **line draft** option to plot Raman spectra.

   4. Utilize the **Peak analyzer** tool to set the baseline of the spectra.

   5. Apply the **Signal process - Smooth** function to smooth the spectra for final results.

Representative Results

A unique method for creating microchannel patterns on nanopaper has been devised utilizing the practical plastic micro-molds through the convenient microembossing technique. Notably, this method accomplishes microchannel patterning at a scale as small as 200 µm, which represents a fourfold improvement compared to existing methods[32,33,34]. After fine-tuning the patterning parameters, the provided guidelines exhibit excellent repeatability in the fabrication process, characterized by minimal standard deviations. The highest observed variation in width is merely 2.5%, while for depth, it is 9%. Additionally, **Figure 2E,F** has been included to serve as a guide for application development.

To demonstrate the practical applications of the developed SERS-NanoPADs, Rhodamine B (RhB), a common environmental pollutant and low-toxicity organic chemical, was selected as an example. RhB molecules were directly mixed with ethanol. In this example, 5 µL of the analyte solution was filled into the inlet zone of NanoPADs, and the Raman signal in the reaction zone was then measured. The Raman spectra of RhB samples at various concentrations in ethanol (ranging from 0.1 pM to 10 µM) are shown in **Figure 5A**, with pure ethanol used as the blank control. Clear RhB bands are observed in the measured spectra, including the C-O-C stretching (1280 cm^{-1}), xanthene ring puckering mode (1200 cm^{-1}), C-N stretching (1384 cm^{-1}), C-C stretching (1350 cm^{-1}), C-H stretching (1520 cm^{-1}), and aromatic C-C stretching (1646 cm^{-1})[40,41]. Due to the sensitivity of the 1646 cm^{-1} peak intensity to RhB concentration with minimal background noise, it was chosen as the reading parameter[42]. The calculation of the limit of detection (LOD) involved determining the RhB concentration corresponding to the intensity of the blank control plus three times the standard deviation of the Raman intensity of the blank control. This calculation yielded a LOD of 0.019 pM. **Figure 5B** displays the calibration curve for RhB detection.

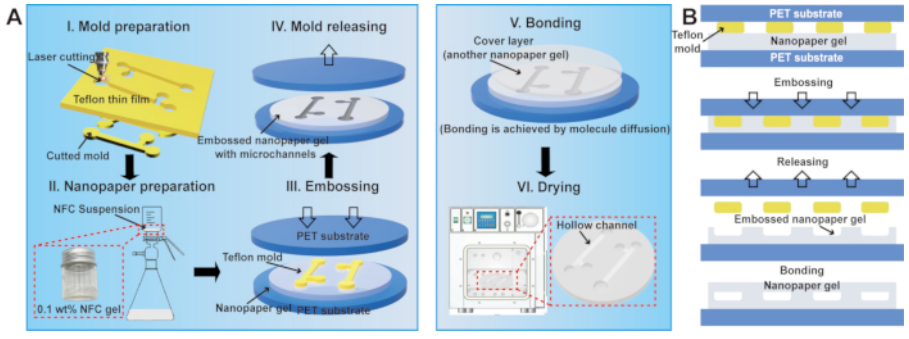

Figure 1: Schematic representation of the microembossing process for patterning microchannels on nanopaper. (**A**) The microembossing process comprises six steps: mold preparations, nanopaper filtration, embossing, mold releasing, bonding, and final drying. (**B**) Cross-sectional view of the microembossing process. The figure is reproduced with permission from Yuan et al. Copyright 2023 American Chemical Society[12]. Please click here to view a larger version of this figure.

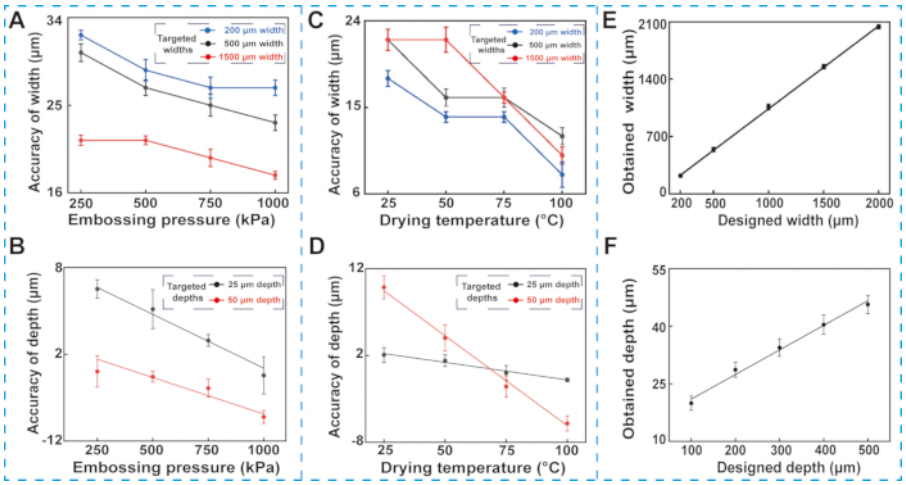

Figure 2: Microchannel embossing optimization. The fabrication accuracy of widths and depths is affected by (**A,B**) embossing pressure and (**C,D**) drying temperature, respectively. Design requirements for (**E**) channel widths and (**F**) depths in nanopaper microfluidic devices (n = 5). (The targeted: the widths and depths of microchannel expected; the obtained: the widths and depths of microchannels fabricated; the designed: the widths and depths of PTFE molds). The figure is reproduced with permission from Yuan et al. Copyright 2023 American Chemical Society[12]. Please click here to view a larger version of this figure.

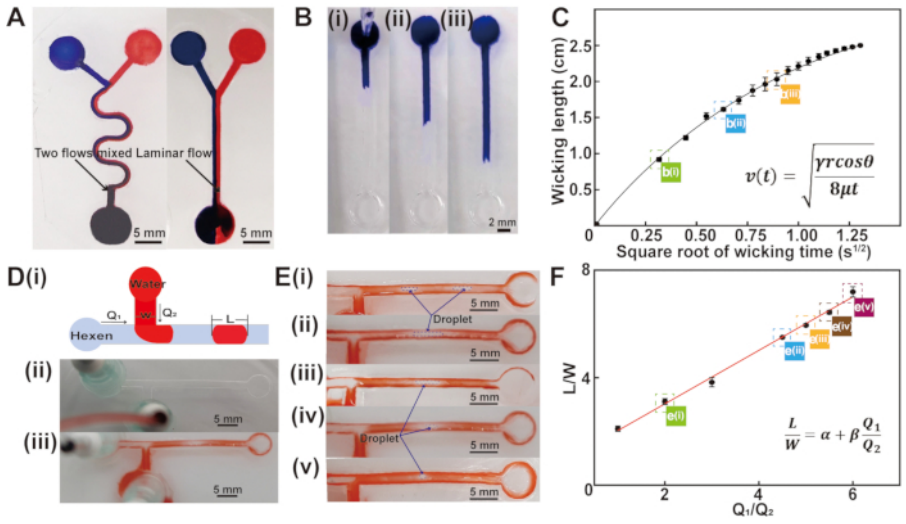

Figure 3: Fundamentals of fluidic behavior in the nanopaper microchannel. (**A**) Photographs of the nanopaper microfluidic mixer and laminar flow device. Scale bars = 5 mm. (**B**) Flow-wicking at different distances along the hollow channel. Scale bar = 2 mm. (**C**) Capillary performance along the hollow channel (n=5). (**D**) Schematic illustration of the droplets inside the T-junction channel and the embossed device with the inlet tubes. (**E**) Droplet generator working at different frequencies. Scale bars = 5 mm. (**F**) Linear dependence on the flow rates of Q_1/Q_2 and L/W (n = 5). The figure is reproduced with permission from Yuan et al. Copyright 2023 American Chemical Society[12]. Please click here to view a larger version of this figure.

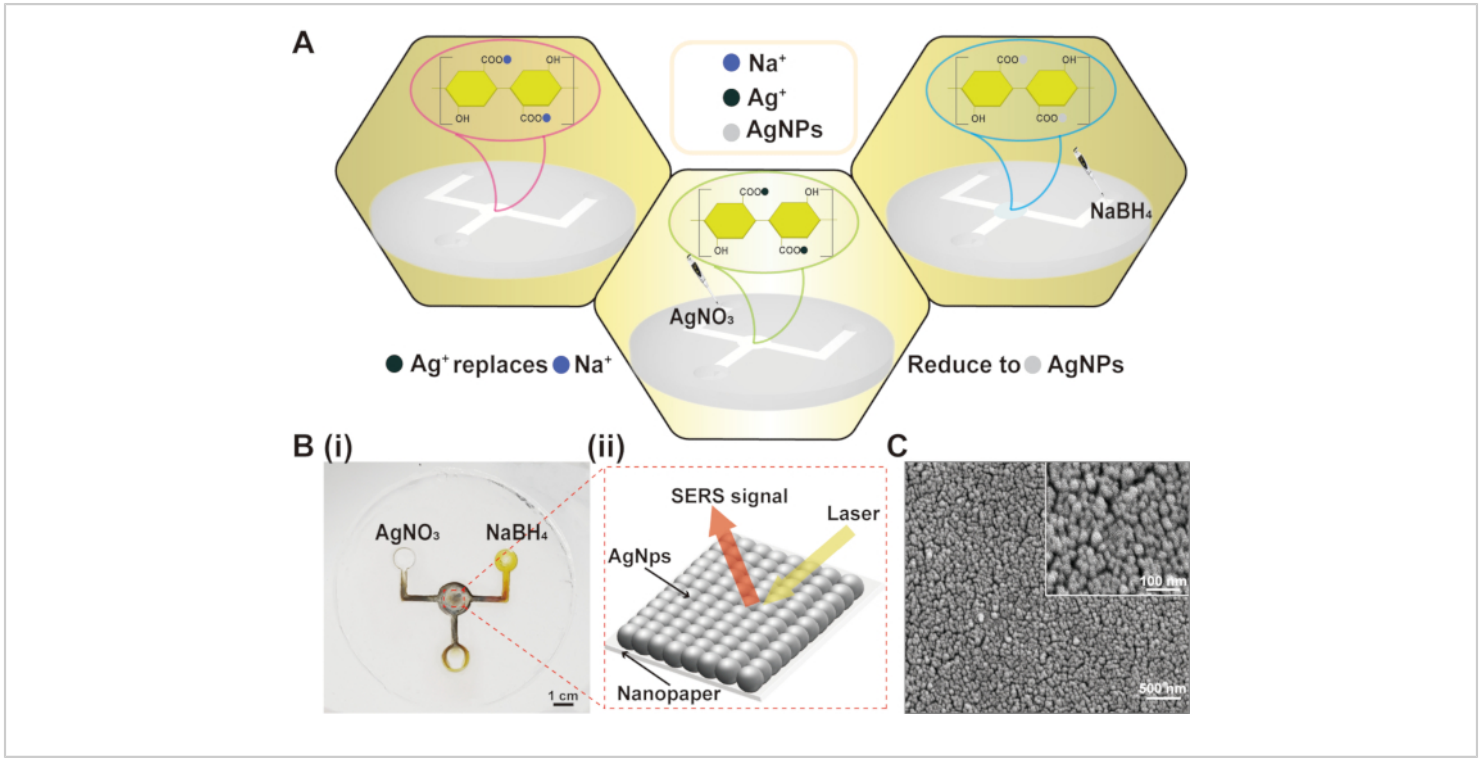

Figure 4: Sensitive SERS sensing of small molecules on NanoPADs. (**A**) Schematic of AgNP growth on the detection zone of the NanoPADs. (**B**) Photograph of NanoPADs after AgNPs growth and schematic of the SERS-based molecule detection. Scale bar = 1 cm. (**C**) SEM image of the *in-situ* grown AgNPs on NanoPADs shows a dense and organized AgNPs array. Scale bar = 500 nm; inset = 100 nm. The figure is reproduced with permission from Yuan et al. Copyright 2023 American Chemical Society[12]. Please click here to view a larger version of this figure.

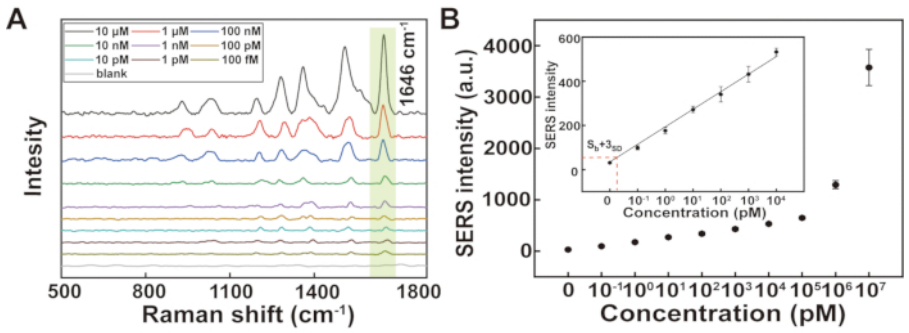

Figure 5: SERS-based detection of RhB. (**A**) Raman spectra of RhB at concentrations of 0.1 pM to 10 μM. (**B**) Calibration of RhB at 1646 cm^{-1} (n=5). The figure is reproduced with permission from Yuan et al. Copyright 2023 American Chemical Society[12]. Please click here to view a larger version of this figure.

Discussion

The primary focus of this study is to develop a simple method for fabricating microchannels on nanopaper. An efficient embossing technique was devised using PTFE as the mold to address this challenge[12]. By optimizing the temperature and embossing pressure, a series of experiments were conducted to establish a reliable fabrication process for NanoPADs. Additionally, the use of a quick-reference table to adjust the applications of NanoPADs in different fields was demonstrated. Although this method is efficient and stable, some challenges were encountered. Initially, metals were used as molds due to their smoothness, but difficulties arose in removing them from the adhesive nanopaper gel. Ultimately, PTFE was chosen for its nonstick properties and ease of operation in the embossing process. Another challenge addressed was the fabrication of hollow channels. The strong hydrogen bonds in 'gel-like' nanopaper[8] allowed for self-diffusion and adhesion of two layers, resulting in compact bonding without external forces.

While the developed method is straightforward, time-saving, and minimizes contamination when fabricating pump-free microchannels on nanopaper, there are still limitations. The precision of laser cutting restricts the width of PTFE molds to 200 μm, consequently limiting the achievable precision of the microchannels to 200 μm. To overcome this limitation, implementing a nano printer for 3D printing molds is planned in future endeavors, leveraging its capacity to achieve a precision of 50 μm. Another area that requires further improvement is the fabrication of 3D microchannels. While 3D microchannels[33,34] have found extensive use in biomedical, chemical, and electrical detection using materials like PDMS and regular paper-based devices, the fabrication of 3D microchannels on nanopaper is still an emerging field. Resolving this challenge will significantly contribute to the advancement of NanoPADs.

This study focused on using molecules as Raman reporters for SERS detection. SERS technology[42] offers numerous advantages, including minimal reagent usage, high selectivity, simple sample preparation, and excellent stability,

making it a crucial method for biochemical detection. The designed NanoPADs have potential applications in SERS immunoassays. Furthermore, there is increasing interest in selective and tailored SERS plasmons. Exploring methods to generate these plasmons on NanoPADs for selective SERS detection represents an exciting avenue for future development in the field of nanopaper.

Disclosures

The authors have nothing to disclose.

Acknowledgments

The authors acknowledge the financial support from the programs of the Natural Science Foundation of the Jiangsu Higher Education (22KJB460033), and Jiangsu Science and Technology Programme - Young Scholar (BK20200251). This work is also partially supported by the XJTLU AI University Research Centre, Jiangsu Province Engineering Research Centre of Data Science and Cognitive Computation at XJTLU and SIP AI innovation platform (YZCXPT2022103). The support from State Key Laboratory for Manufacturing Systems Engineering via the open project (SKLMS2023019) and Key Laboratory of Bionic Engineering, Ministry of Education, are also acknowledged.

References

1. Zhu, H., Fang, Z., Preston, C., Li, Y., Hu, L. Transparent paper: fabrications, properties, and device applications. *Energy & Environmental Science.* **7** (1), 269-287 (2013).
2. Nogi, M., Iwamoto, S., Nakagaito, A. N., Yano, H. Optically transparent nanofiber paper. *Advanced Materials.* **21** (16), 1595-1598 (2009).
3. Li, X. et al. Three-dimensional sulfated bacterial cellulose/gelatin composite scaffolds for culturing hepatocytes. *Cyborg and Bionic Systems.* **4**, 0021 (2023).
4. Barhoum, A., Samyn, P., Öhlund, T., Dufresne, A. Review of recent research on flexible multifunctional nanopapers. *Nanoscale.* **9** (40), 15181-15205 (2017).
5. Dufresne, A. Nanocellulose: a new ageless bionanomaterial. *Materials Today.* **16** (6), 220-227 (2013).
6. Martin-Martinez, F. J. Designing nanocellulose materials from the molecular scale. *Proceedings of the National Academy of Sciences.* **115** (28), 7174-7175 (2018).
7. Sehaqui, H., Liu, A., Zhou, Q., Berglund, L. A. Fast preparation procedure for large, flat cellulose and cellulose/inorganic nanopaper structures. *Biomacromolecules.* **11** (9), 2195-2198 (2010).
8. Fang, Z. et al. Novel nanostructured paper with ultrahigh transparency and ultrahigh haze for solar cells. *Nano Letters.* **14** (2), 765-773 (2014).
9. Zheng, G. et al. Nanostructured paper for flexible energy and electronic devices. *MRS Bulletin.* **38** (4), 320-325 (2013).
10. Chen, L., Ying, B., Song, P., Liu, X. A nanocellulose-paper-based sers multiwell plate with high sensitivity and high signal homogeneity. *Advanced Materials Interfaces.* **6** (24), 1901346 (2019).
11. Koga, H. et al. Transparent, conductive, and printable composites consisting of tempo-oxidized nanocellulose and carbon nanotube. *Biomacromolecules.* **14** (4), 1160-1165 (2013).
12. Yuan, W. et al. Facile microembossing process for microchannel fabrication for nanocellulose-paper-based

microfluidics. *ACS Applied Materials & Interfaces.* **15** (5), 6420-6430 (2023).

13. Rolland, J. P., Mourey, D. A. Paper as a novel material platform for devices. *MRS Bulletin.* **38** (4), 299-305 (2013).
14. Martinez, A. W., Phillips, S. T., Butte, M. J., Whitesides, G. M. Patterned paper as a platform for inexpensive, low-volume, portable bioassays. *Angewandte Chemie International Edition.* **46** (8), 1318-1320 (2007).
15. Chin, C. D., Linder, V., Sia, S. K. Lab-on-a-chip devices for global health: past studies and future opportunities. *Lab on a Chip.* **7** (1), 41-57 (2006).
16. Chin, C. D. et al. Microfluidics-based diagnostics of infectious diseases in the developing world. *Nature Medicine.* **17** (8), 1015-1019 (2011).
17. Martinez, A. W., Phillips, S. T., Whitesides, G. M., Carrilho, E. Diagnostics for the developing world: microfluidic paper-based analytical devices. *Analytical Chemistry.* **82** (1), 3-10 (2010).
18. Carrilho, E., Martinez, A. W., Whitesides, G. M. Understanding wax printing: a simple micropatterning process for paper-based microfluidics. *Analytical Chemistry.* **81** (16), 7091-7095 (2009).
19. Lu, Y., Shi, W., Qin, J., Lin, B. Fabrication and characterization of paper-based microfluidics prepared in nitrocellulose membrane by wax printing. *Analytical Chemistry.* **82** (1), 329-335 (2010).
20. Li, X., Zhao, C., Liu, X. A paper-based microfluidic biosensor integrating zinc oxide nanowires for electrochemical glucose detection. *Microsystems & Nanoengineering.* **1** (1), 1-7 (2015).
21. Nie, Z. et al. Electrochemical sensing in paper-based microfluidic devices. *Lab on a Chip.* **10** (4), 477-483 (2010).
22. Cai, T. et al. A paper-based microfluidic analytical device with a highly integrated on-chip valve for autonomous ELISA. *2022 IEEE 35th International Conference on Micro Electro Mechanical Systems Conference (MEMS).* 271-274 (2022).
23. Murdock, R. C. et al. Optimization of a paper-based ELISA for a human performance biomarker. *Analytical Chemistry.* **85** (23), 11634-11642 (2013).
24. Cheng, C. M. et al. Paper-based ELISA. *Angewandte Chemie.* **122** (28), 4881-4884 (2010).
25. Holstein, C. A. et al. Immobilizing affinity proteins to nitrocellulose: a toolbox for paper-based assay developers. *Analytical and Bioanalytical Chemistry.* **408** (5), 1335-1346 (2016).
26. Tenda, K. et al. Paper-based antibody detection devices using bioluminescent bret-switching sensor proteins. *Angewandte Chemie International Edition.* **57** (47), 15369-15373 (2018).
27. Gong, M. M., Nosrati, R., San Gabriel, M. C., Zini, A., Sinton, D. Direct DNA Analysis with paper-based ion concentration polarization. *Journal of the American Chemical Society.* **137** (43), 13913-13919 (2015).
28. Gan, W. et al. A filter paper-based microdevice for low-cost, rapid, and automated DNA extraction and amplification from diverse sample types. *Lab on a Chip.* **14** (19), 3719-3728 (2014).
29. Liu, Y. et al. Fluorescent paper-based analytical devices for ultra-sensitive dual-type RNA detections and accurate

gastric cancer screening. *Biosensors and Bioelectronics.* **197**, 113781 (2022).

30. Yuan, H. et al. Microfluidic-assisted *Caenorhabditis elegans* sorting: current status and future prospects. *Cyborg and Bionic Systems.* **4**, 0011 (2023).
31. Kim, H. et al. Origami-paper-based device for microvesicle/exosome preconcentration and isolation. *Lab on a Chip.* **19** (23), 3917-3921 (2019).
32. Ying, B. et al. NanoPADs and nanoFACEs: an optically transparent nanopaper-based device for biomedical applications. *Lab on a Chip.* **20** (18), 3322-3333 (2020).
33. Shin, S., Hyun, J. Matrix-assisted three-dimensional printing of cellulose nanofibers for paper microfluidics. *ACS Applied Materials & Interfaces.* **9** (31), 26438-26446 (2017).
34. Browne, C., Garnier, G., Batchelor, W. Moulding of micropatterned nanocellulose films and their application in fluid handling. *Journal of Colloid and Interface Science.* **587**, 162-172 (2021).
35. Paul, R. et al. Shear stress related blood damage in laminar couette flow. *Artificial Organs.* **27** (6), 517-529 (2003).
36. Thuo, M. M. et al. Fabrication of low-cost paper-based microfluidic devices by embossing or cut-and-stack methods. *Chemistry of Materials.* **26** (14), 4230-4237 (2014).
37. Garstecki, P., Fuerstman, M. J., Stone, H. A., Whitesides, G. M. Formation of droplets and bubbles in a microfluidic T-junction-scaling and mechanism of break-up. *Lab on a Chip.* **6** (3), 437-446 (2006).
38. Nisisako, T., Torii, T., Higuchi, T. Droplet formation in a microchannel network. *Lab on a Chip.* **2** (1), 24-26 (2002).
39. Wang, Y., Zhang, X., Wen, G., Liang, A., Jiang, Z. Facile synthesis of a highly SERS active nanosilver sol using microwaves and its application in the detection of E. coli using Victoria blue B as a molecular probe. *Analytical Methods.* **8** (24), 4881-4887 (2016).
40. Pham, T. T. H., Dien, N. D., Vu, X. H. Facile synthesis of silver/gold alloy nanoparticles for ultra-sensitive rhodamine B detection. *RSC Advances.* **11** (35), 21475-21488 (2021).
41. Li, D., Li, D. W., Li, Y., Fossey, J. S., Long, Y. T. Cyclic electroplating and stripping of silver on Au@SiO2 core/shell nanoparticles for sensitive and recyclable substrate of surface-enhanced Raman scattering. *Journal of Materials Chemistry.* **20** (18), 3688-3693 (2010).
42. Sun, C. H., Wang, M. L., Feng, Q., Liu, W., Xu, C. X. Surface-enhanced Raman scattering (SERS) study on Rhodamine B adsorbed on different substrates. *Russian Journal of Physical Chemistry A.* **89** (2), 291-296 (2015).